MCB
Journals.ASM.org

Angiogenin-Cleaved tRNA Halves Interact with Cytochrome *c*, Protecting Cells from Apoptosis during Osmotic Stress

Mridusmita Saikia,[a] Raul Jobava,[b] Marc Parisien,[c] Andrea Putnam,[b,d] Dawid Krokowski,[a] Xing-Huang Gao,[a] Bo-Jhih Guan,[a] Yiyuan Yuan,[a] Eckhard Jankowsky,[b,d] Zhaoyang Feng,[a] Guo-fu Hu,[e] Marianne Pusztai-Carey,[b] Madhavi Gorla,[f] Naresh Babu V. Sepuri,[f] Tao Pan,[c] Maria Hatzoglou[a]

Departments of Pharmacology[a] and Biochemistry[b] and Center for RNA Molecular Biology,[d] Case Western Reserve University, Cleveland, Ohio, USA; Department of Biochemistry and Molecular Biology, University of Chicago, Chicago, Illinois, USA[c]; Molecular Oncology Research Institute, Tufts Medical Center, Boston, Massachusetts, USA[e]; Department of Biochemistry, School of Life Sciences, University of Hyderabad, Hyderabad, Andhra Pradesh, India[f]

Adaptation to changes in extracellular tonicity is essential for cell survival. However, severe or chronic hyperosmotic stress induces apoptosis, which involves cytochrome *c* (Cyt *c*) release from mitochondria and subsequent apoptosome formation. Here, we show that angiogenin-induced accumulation of tRNA halves (or tiRNAs) is accompanied by increased survival in hyperosmotically stressed mouse embryonic fibroblasts. Treatment of cells with angiogenin inhibits stress-induced formation of the apoptosome and increases the interaction of small RNAs with released Cyt *c* in a ribonucleoprotein (Cyt *c*-RNP) complex. Next-generation sequencing of RNA isolated from the Cyt *c*-RNP complex reveals that 20 tiRNAs are highly enriched in the Cyt *c*-RNP complex. Preferred components of this complex are 5′ and 3′ tiRNAs of specific isodecoders within a family of isoacceptors. We also demonstrate that Cyt *c* binds tiRNAs *in vitro*, and the pool of Cyt *c*-interacting RNAs binds tighter than individual tiRNAs. Finally, we show that angiogenin treatment of primary cortical neurons exposed to hyperosmotic stress also decreases apoptosis. Our findings reveal a connection between angiogenin-generated tiRNAs and cell survival in response to hyperosmotic stress and suggest a novel cellular complex involving Cyt *c* and tiRNAs that inhibits apoptosome formation and activity.

Cellular stress initiates a complex cascade of signaling pathways in an attempt to return the cell to its previous equilibrium. In most cases, the type, duration, and intensity of stress govern the outcome of the cellular response, resulting in either adaptation or cell death. Apoptosis is induced if the damage that occurred during stress exceeds the capacity of the repair mechanisms.

In vertebrates, apoptosis is orchestrated through one of two signaling cascades, termed the intrinsic and extrinsic apoptotic pathways (1). Both pathways converge at the activation of executioner caspase proteins 3 and 7 (1). These caspases signal the onset of apoptosis via cleavage of numerous cellular proteins, ultimately leading to the phagocytic recognition and engulfment of the dying cell (1). Mitochondria play a critical role in mediating the intrinsic apoptotic signal transduction pathway. During apoptosis mitochondria undergo biochemical and structural changes, which include swelling, depolarization, increased permeability of the outer membrane, and release of proteins from the intermembrane space, including cytochrome *c* (Cyt *c*) (2, 3). The released Cyt *c* binds the apoptotic protease activating factor 1 protein (Apaf-1) in the cytoplasm (4). This causes a conformational change and oligomerization of Apaf-1 that leads to the formation of the caspase activation platform, the apoptosome (5). The apoptosome recruits and activates initiating caspase 9, which in turn cleaves and activates caspase 3 (1).

The formation of the macromolecular complex apoptosome is a key event in the intrinsic apoptotic pathway. The binding of Cyt *c* to Apaf-1 is regulated through the action of various proteins (3), cations, and nucleotides (6, 7). Disruption of the binding of Cyt *c* to Apaf-1 can block the formation of the apoptosome and the subsequent activation of caspase 9, thus leading to inhibition of apoptosis (8, 9).

Apoptosis is the underlying mechanism of several diseases, such as organ failure and neurodegeneration as in amyotrophic lateral sclerosis (10, 11). Efforts have been directed toward the discovery of molecules that can attenuate apoptosis-mediated cell loss in disease states (10). Recent reports suggest that angiogenin (ANG) protects motor neurons from death induced by various cellular stresses, including excitotoxicity and hypoxia (12–14). The mechanism of this protective action of ANG in neurons remains largely unknown. ANG belongs to the pancreatic RNase A superfamily, a protein that cleaves single-stranded RNA (15). Widespread expression of ANG suggests that it may play a more universal role in the cell than stimulating angiogenesis (16, 17). An interesting function of ANG under certain stress conditions is tRNA cleavage at the anticodon loop, leading to an accumulation of small tRNA halves, known as tiRNAs (18–24).

We have previously shown that hyperosmotic stress induces apoptosis in wild-type mouse embryonic fibroblasts (MEFs) following the release of Cyt *c* from mitochondria (25). Hyperosmotic stress causes cell shrinkage, thus increasing macromolecular crowding and inducing a stress response (26). Regulation of cell volume and adaptation to hyperosmotic stress are fundamental processes required for the maintenance and well-being of all living cells (26). In a recent study, we showed that hyperosmotic stress induces tiRNA accumulation as early as 15 min after exposure to stress (20). The generation of tiRNAs during hyperosmotic stress

Received 26 January 2014 **Returned for modification** 12 February 2014
Accepted 11 April 2014
Published ahead of print 21 April 2014
Address correspondence to Maria Hatzoglou, mxh8@case.edu.
M.S., R.J., M.P., A.P., and D.K. contributed equally to this article.

doi:10.1128/MCB.00136-14

was shown to be regulated by various factors, including the rate of protein synthesis, the availability of free tRNAs, and the activation of ANG (20). Interestingly, tiRNA accumulation preceded Cyt *c* release from mitochondria, igniting the idea that there may be a functional significance for the temporal accumulation of tiRNAs in the cytoplasm of stressed cells. An important reported function of tiRNAs in the cellular stress response is the inhibition of protein synthesis (18, 21, 27). However, the kinetics of accumulation of bulk tiRNAs during hyperosmotic stress did not correlate with the pattern of inhibition of protein synthesis (20), suggesting that subpopulations of tiRNAs generated from different tRNA isoacceptors and isodecoders may influence different cellular processes, including protein synthesis rates.

In this study, we tested the hypothesis that addition of ANG into cells exposed to hyperosmotic stress is cytoprotective, generating a population of tiRNAs via its tRNA cleavage action. During early hyperosmotic stress, treatment of MEFs with ANG caused a decrease in caspase 3 activity and an increase in cell viability. ANG treatment of MEFs during stress also inhibited the recruitment of Apaf-1 into the apoptosome. We therefore propose a mechanism whereby tiRNAs in the cytoplasm can form complexes with Cyt *c* freshly released from mitochondria. This event either sequesters Cyt *c* away from binding to Apaf-1 or interferes with formation of the apoptosome and the downstream cleavage of caspase 3. We have performed deep-sequencing experiments on 30- to 45-nucleotide (nt) RNAs isolated before and after Cyt *c* immunoprecipitation (IP) to show that Cyt *c* forms complexes preferentially with a small group of tiRNAs during stress. A recent report demonstrated that apoptosome formation *in vitro* was inhibited by the addition of *in vitro*-synthesized full-length tRNAs (28–30). However, to the best of our knowledge, there are no reports on the function of endogenous cellular tRNAs or tiRNAs in apoptosome formation and activity under physiologically relevant conditions. So far, studies of the tRNA's role in apoptosome formation have been performed in cell extracts or via exogenous transfection of tRNAs. Our study here provides *in vivo* evidence of the existence of a ribonucleoprotein particle (RNP) made up of at least Cyt *c* with tRNA-derived small RNA molecules, all in a biologically relevant context. We also show *in vivo* that under stress conditions Cyt *c* preferentially binds to tiRNAs and not tRNAs, a welcome feature given the very low availability of free tRNAs in the cell. We conclude that ANG guards cells during cellular stress by inhibiting the activation of the apoptosis pathway. The proposed cytoprotective mechanism is that early tiRNA generation and accumulation titrate out released Cyt *c* from compromised mitochondria. This opens up the possibility of ANG usage as a therapeutic agent.

MATERIALS AND METHODS

Bioinformatic analysis. Sequences were aligned on the *Mus musculus* genome, partly provided in a GenBank flat file (ftp://ftp.ncbi.nlm.nih.gov/genomes/M_musculus/RNA/) and partly from the Genomic tRNA Database, data set mm10 (http://gtrnadb.ucsc.edu/Mmusc10/) (31). The reads were aligned with an in-house aligner allowing at most one mismatch and no insertion/deletion (indel) with the targeted genes. Hits with the longest alignments were retained. A mountain plot of each tRNA gene was made by accumulating the reads that map to the gene, with the height of the mountain for a gene position indicating the number of times that that position was covered by reads. The enrichment plot is two mountain plots, one on top of another. Here, we used low-frequency Fourier transforms to smooth the plots. In the plots shown in Fig. 4 and 5, red vertical bars indicate peaks of the smoothed curves, and their heights are proportional to the enrichment values between the two curves. The curves are normalized by the number of reads per kilobase per million mapped reads (rpkM) in their own set.

Caspase 3 activity assay. The activity of caspase 3 was determined by measuring the rate of cleavage of the specific fluorescent substrate (Asp-Glu-Val-Asp–7-amido-4-trifluoromethylcoumarin [AFC]) (Calbiochem/Millipore). Activated caspase 3 cleaves this substrate, generating highly fluorescent AFC that can be detected using a fluorescence reader with excitation at 360 nm and emission between 420 and 460 nm (ThermoMax microplate reader; Molecular Devices). The amount of AFC produced is proportional to the caspase 3 activity in the samples. A total of 1×10^5 cells were seeded into a 96-well microplate for 16 h prior to treatments. Cells were lysed in extraction buffer containing HEPES (10 mM), CHAPS {3-[(3-cholamidopropyl)-dimethylammonio]-1-propanesulfonate; 1%}, NaCl (150 mM), SDS (0.1%), dithiothreitol (DTT; 1 mM), and EDTA (1 mM) before the addition of the substrate (100 μM). The reaction mixture was then incubated at 37°C for 1 h.

Caspase 9 activity assay. The caspase 9 activity was measured in cell extracts by the cleavage of the fluorescent substrate Leu-Glu-His-Asp (LEHD)-AFC (EMD, Millipore) and release of free AFC, which emits a yellow-green fluorescence (lambda maximum of 505 nm). An M3 microplate reader then quantified the fluorescence intensity. MEFs were extracted in lysis buffer (20 mM HEPES-NaOH, pH 7.4, 0.1% CHAPS, 2 mM EDTA, 10% sucrose, 100 mM NaCl) with protease and phosphatase inhibitors (Roche) for 10 min on ice. Insoluble cell debris was removed by centrifugation at 15,000 × *g* for 15 min. Cell lysates (200 μg/sample) were added in the reaction buffer (0.1 mM LEHD-AFC, 50 mM Tris-HCl, pH 7.2, 1 mM EDTA, 5 mM DTT, 10% sucrose, and 0.1% CHAPS) and incubated at 37°C. Changes in fluorescence intensity were expressed as mU/min/mg protein.

Cell culture. MEFs were cultured in high-glucose Dulbecco's modified Eagle's medium supplemented with 10% fetal bovine serum, 2 mM glutamine, 100 units/ml penicillin, and 100 μg/ml streptomycin. Medium was supplemented with sucrose to give the desired osmolality as previously described (25). Unless otherwise specified, hyperosmotic medium was 600 mosmol/liter obtained by addition of 300 mM sucrose to standard medium. MEFs were pretreated with 0.5 μg/ml recombinant ANG (R&D Systems) for 30 min and then in combination with the hyperosmotic medium for ANG plus hyperosmotic treatments. Cortical neurons were prepared from C57BL/6J pups as previously described (25). All animal studies were conducted according to the *Guide for the Care and Use of Laboratory Animals* (55) and approved by the Institutional Animal Care and Use Committee at Case Western Reserve University.

Cell viability assays. Cells were grown in six-well plates and incubated until they achieved approximately 70 to 80% confluence at the time of treatments. Following the indicated treatments (see Fig. 1E and 7C) and detachment by trypsin, cells were suspended in phosphate-buffered saline (PBS). Muse cell count and viability reagent (Millipore) was added, and the cell suspension was incubated at room temperature for 5 min. Cell viability was determined by using a Muse cell analyzer (Millipore) according to the manufacturer's protocol.

Electrophoretic mobility shift assays. We used two methodologies to perform RNA-Cyt *c* binding reactions and electrophoretic mobility shift assays. (i) For the experiments shown in Fig. 6A to C, reaction mixtures (10 μl) contained 40 mM HEPES (pH 7.5), 30 mM KCl, 2 mM $MgCl_2$, 5% glycerol, 1 unit/μl RNasin, 1 nM radiolabeled tiRNA or pooled tiRNA-containing RNA (tiRNA*^{pool} immunoprecipitated with Cyt *c*), and the indicated concentrations (see Fig. 6A to C) of Cyt *c* (Sigma) (stored in 50 mM phosphate buffer [pH 7.5]). Reaction mixtures were incubated for 30 min at 30°C. Reaction products were applied to an 8% nondenaturing polyacrylamide-bis gel (79:1), which was run at 4°C. Gels were dried, and radiolabeled RNAs were visualized with a Typhoon PhosphorImager (Amersham Biosciences). The fraction of bound RNA was quantified using ImageQuant, version 5.2, software (Molecular Dynamics). RNA binding curves were fit to the following equation: $F = F_{max} \times$

[Cyt *c*]/($K_{1/2}$ + [Cyt *c*]), where *F* is the fraction of RNA bound, F_{max} is the fraction of RNA bound at Cyt *c* saturation, and $K_{1/2}$ is the apparent affinity of Cyt *c* to the RNA. Cyt *c* binding reached saturation at an F_{max} of 0.14, and this value was used to calculate all apparent affinities. The tiRNA sequences were as follows: 5′ tiRNA^{Asp}-GUC, 5′-pUCCUCGUUAGUAU AGUGGUGAGUAUCCCUGCCU-3′; 3′ tiRNA^{Arg}-ACG, 5′-GGAUCAG AAGAUUCUAGGUUCGACUCCUGGCUGGCUCGCCA-3′; 3′ tiRNA^{Gly}-UCC, 5′-CCAAGCAGUUGACCCGGGUUCGAUUCCCGGCCAACGCAC CA-3′; 3′ tiRNA^{Ile}-UAU, 5′-UAAUGCCGAGGUUGUGAGUUCGAGCCUC ACCUGGAGCACCA-3′; 3′ tiRNA^{Thr}-CGU/UGU, 5′-UAAACAGGAGAUCC UGGGUUCGAAUCCCAGUGGGGCCUCCA-3′; 3′ tiRNA^{Ala}-AGC, 5′-UG CACGAGGCCCCGGGUUCAAUCCCCGGCACCUCCACCA-3′; and yeast tRNA-^{Met}, 5′-GGCGCCGUGGCGCAGUGGAAGCGCGCAGGG-CUCA UAACCCUGAUGUCCUCGGAUCGAAACCGAGCGGCGCUA-3′. (ii) For the experiments shown in Fig. 6D to F, reactions were performed as previously described (32). Briefly, RNA-binding reaction mixtures were incubated in 20 mM Tris-HCl, pH 7.0, and 5 mM $MgCl_2$ at 30°C for 45 min. After incubation, the reaction was quenched by the addition of 5× loading dye (50% glycerol and 1 mg/ml xylene cyanol), and protein-RNA complexes were separated by 12% nondenaturing PAGE, followed by staining with methylene blue (0.1 M sodium acetate and 0.02% methylene blue) for 1 h at room temperature. Gels were destained overnight with autoclaved Milli Q water.

Gel filtration assay. Gel filtration analysis was performed on a Superose 6 10/300 GL prepacked Tricorn column for high-performance gel filtration (GE Healthcare Life Sciences, Pittsburgh, PA), attached to a Waters 1525 binary high-performance liquid chromatography (HPLC) system, equipped with a 2489 dual-wavelength UV/visible light detector (Waters Corporation, Milford, MA). The column was calibrated with a mixture of molecular mass standards in the range of 14 to 700 kDa. Cell extracts (3.5 mg) in a buffer consisting of 50 mM Tris-HCl, pH 7.6, 50 mM NaCl, 1 mM phenylmethylsulfonyl fluoride (PMSF), and 1 mM DTT were loaded on the column at a 0.5 ml/min flow rate, and 1-ml fractions were collected every 2 min. The total protein in each fraction was precipitated using trichloroacetic acid (TCA) and used for Western blot analysis.

Immunoprecipitations. MEFs were subjected to combined ANG and hyperosmotic treatment as specified above. Total cell extracts (500 μg of total protein) were immunoprecipitated with 5 μg of Cyt *c* antibody (BD Pharmingen) as described previously (33).

Isolation and labeling of tRNA fragments. Total RNA enriched in small RNAs was obtained using a mirVana miRNA isolation kit (Life Technologies) according to the manufacturer's protocol. Total RNA (5 μg) was 5′ end labeled with [γ-^{32}P]ATP and was separated on 10% Tris-borate-EDTA (TBE)–urea polyacrylamide gels. RNA sequencing was performed by BGI Americas.

Lentivirus production. Lentiviral particles expressing short hairpin RNAs (shRNAs) and control viruses were prepared in HEK293T cells according to standard procedures. Briefly, cells were transfected with either plasmid (pLKO.1) or plasmid expressing a shRNA against ANG1 (Open Biosystems), and medium was collected 24 h after transfection over a period of 3 days and filtered through a 0.45-μm-pore-size membrane. Viral particles were concentrated by ultracentrifugation (3 h at 25,000 rpm) through a 20% sucrose cushion and dissolved in Hanks balanced salt solution (HBSS). MEFs were infected in the presence of Polybrene (10 μg/ml), and selection of infected cells with puromycin was performed 24 h after infection over a period of 5 days. The efficiency of ANG depletion in infected cells was established by Western blotting.

Mitochondrion isolation. Cells were plated into 500-cm^2 dishes and incubated until they achieved approximately 80% confluence at the time of treatments. Following detachment by trypsin, cells were suspended into isolation medium (50 mM mannitol, 50 mM sucrose, 100 mM KCl, 50 mM morpholinepropanesulfonic acid [MOPS], 5.0 mM $MgSO_4$, [pH 7.4]) and incubated for 10 min on ice following 10 to 18 strokes in glass homogenizers. The homogenate was then centrifuged at 550 × *g* for 5 min at 4°C, and the supernatants were centrifuged again at 8,000 × *g* for 10 min to pellet precipitate the mitochondria. The pellet was then washed three times with KME buffer (100 mM KCl, 50 mM MOPS, 0.5 mM EGTA [pH 7.4]). Mitochondrial protein concentrations were determined by the bicinchoninic acid (BCA) method (using a micro-BCA protein assay kit; Thermo-Scientific, Waltham, MA).

RNA sequencing. RNA sequencing was performed at the BGI Americas Corporation. RNA was isolated from Cyt *c* IPs using a mirVana miRNA isolation kit (Life Technologies) according to the manufacturer's protocol. PAGE was used to separate the small RNAs based on their sizes, and gel-purified fractions were used for further analysis. Briefly, 5′ and 3′ adaptors were ligated to the ends of the small RNAs. The ligation products were purified with PAGE. cDNAs were prepared using reverse transcription, followed by PAGE purification. The cDNA libraries were then used in the Illumina sequencing platform.

TUNEL assay. A terminal deoxynucleotidyltransferase-mediated dUTP-biotin nick end labeling (TUNEL) assay was carried out using an *in situ* cell death detection kit (Roche). Cells were washed with PBS three times and then fixed with 4% paraformaldehyde in PBS for 15 min at room temperature. Fixed and washed cells were treated with 0.1% Triton X-100 for 10 min at room temperature and washed with PBS three times. Finally, cells were treated with TUNEL assay reaction mixture at 37°C for 1 h in the dark. Treated cells were then washed with PBS three times and imaged with a fluorescence microscope (Leica DMI 4000B).

Western blotting. Western blot analysis was performed using standard procedures. The following antibodies were obtained from the indicated sources: anti-ANG (Santa Cruz Biotechnology), anti-caspase 3 (Cell Signaling), anti-caspase 9 (MBL International Corporation), anti-MS204 (Abcam), and anti-Cyt *c* (R&D Systems).

Nucleotide sequence accession number. Small RNA sequencing data were deposited in the Gene Expression Omnibus (http://www.ncbi.nih.gov/geo) under accession number GSE57435.

RESULTS

Early ANG treatment protects MEFs from apoptosis during hyperosmotic stress. Severe hyperosmotic stress can induce apoptosis in all cell types (25). We examined the effect of treatment of cells with exogenous ANG on hyperosmotic stress-induced cleavage of the procaspase 3 in MEFs. ANG is a secreted protein and is known to enter cells by endocytosis (34). We hypothesized that ANG treatment would provide protection from apoptosis during hyperosmotic stress. All treatments in this report were in medium of 600 mosmol/liter. In MEFs cultured in hyperosmotic medium, cleavage of procaspase 3 was observed at 1 h, increased at 2 h, and remained constant for the next 3 h of treatment (Fig. 1A). Addition of ANG during hyperosmotic stress delayed cleavage of procaspase 3 during the first 2 h of exposure to stress. The antiapoptotic effect of ANG was not significant at later times (Fig. 1A), suggesting that ANG has a protective effect on apoptosis during the early response to hyperosmotic stress.

The sequence of events leading to apoptosis during the hyperosmotic stress response can vary depending on the nature, duration, and intensity of the stress (25). Early stress events are often guided toward adaptation and include antiapoptotic mechanisms (25, 35). In order to understand the mechanism behind ANG-mediated protection during hyperosmotic stress, we probed the very early kinetics of this phenomenon. MEFs were cultured in hyperosmotic medium for 15 min, 30 min, 1 h, and 2 h in the presence and absence of ANG, and cleavage of procaspase 3 was monitored. It was shown that ANG reduced the cleavage of both procaspase 3 and procaspase 9 (Fig. 1B). These data are in agreement with our previous report that showed an increase in the number of cells with released Cyt *c* from mitochondria at 2 h of

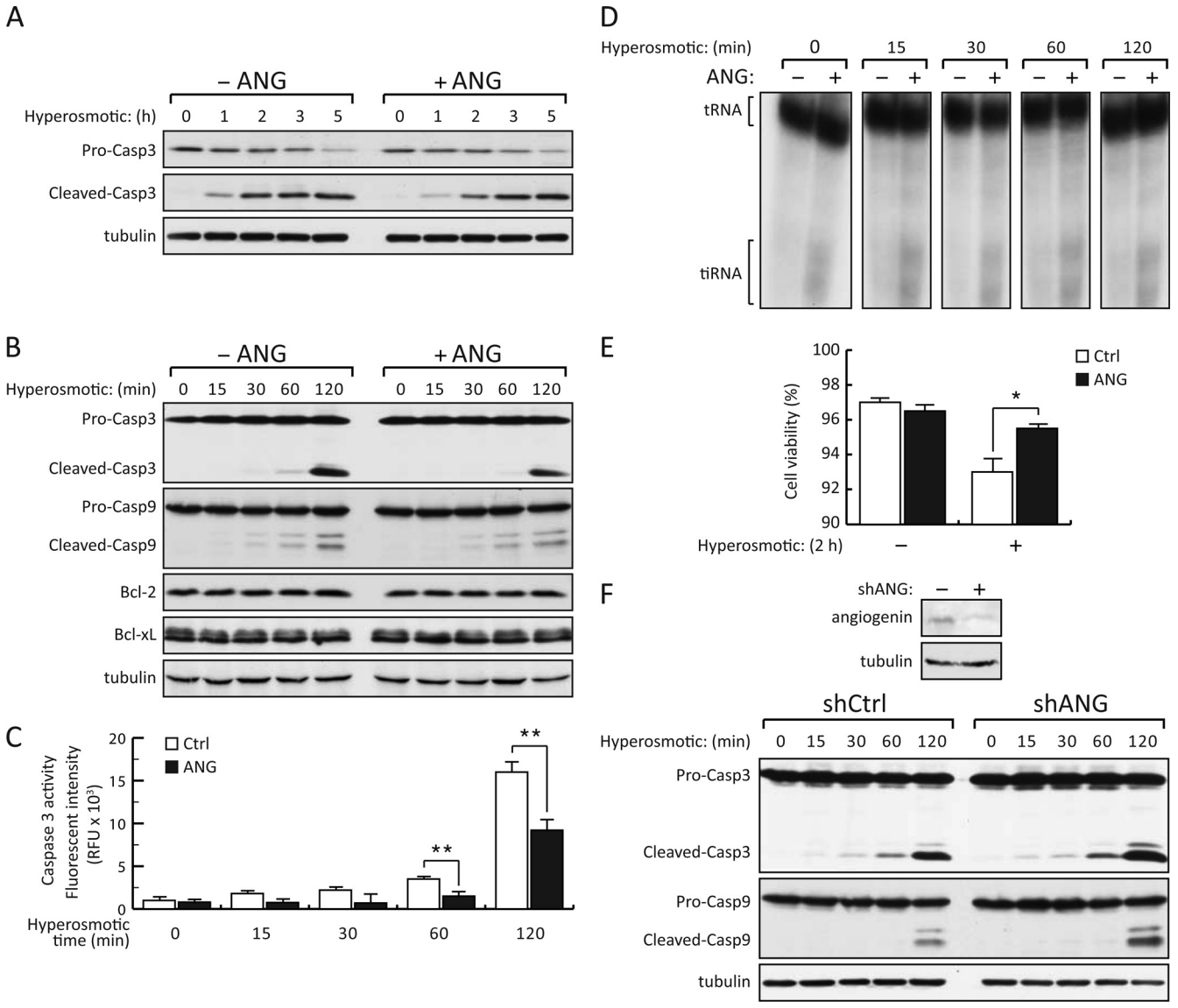

FIG 1 ANG inhibits caspase 3 activity during early hyperosmotic stress. MEFs were incubated in hyperosmotic medium alone or in the presence of ANG (0.5 μg/ml) for the indicated times. (A and B) Western blot analysis of proteins from total cell extracts for the indicated proteins. (C) Caspase 3 activity in cell extracts from three biological replicates for the indicated treatments. (D) Total RNA 5′ end labeled with [γ-^{32}P]ATP was analyzed on 10% urea-polyacrylamide gels. The migrations of tRNAs and tiRNAs are indicated with brackets. (E) Cell viability assays from three biological replicates for the indicated treatments using a Muse cell count and viability kit. (F) Western blot analysis of cell extracts from MEFs treated with ANG-targeted shRNA (shANG) or an shRNA control (shCtrl) for the indicated proteins and the indicated times. The significance of differences among means in panels C and E were evaluated using the Student *t* test (*, $P < 0.05$; **, $P < 0.01$). Error bars represent standard errors.

hyperosmotic stress (25). It was shown previously that increased levels of the antiapoptotic proteins Bcl-2 and Bcl-x_L can inhibit Cyt *c* release from mitochondria (36). Bcl-2 and Bcl-x_L levels remained unchanged throughout the treatment and were not affected by the addition of ANG (Fig. 1B).

To further confirm and quantify the inhibitory effect of ANG on caspase 3 activation and apoptosis, we measured caspase 3 activity in stressed cells (Fig. 1C). ANG treatment significantly decreased caspase 3 activity during hyperosmotic stress treatment in MEFs at the 1-h and 2-h time points (Fig. 1C). At 2 h the caspase 3 activity decreased by 50% in the presence of ANG (Fig. 1C). Interestingly, accumulation of tiRNAs increased at 15 min of ANG treatment and did not increase further during the 2 h of hyperosmotic stress (Fig. 1D), in agreement with our previous report (20). To further support this finding, we performed cell viability assays after 2 h of hyperosmotic stress. Viability was higher for the ANG-treated MEFs (Fig. 1E). The antiapoptotic effect of ANG during hyperosmotic stress was further supported by the increased accumulation of cleaved caspase 3 in MEFs depleted of ANG (Fig. 1F). MEFs infected with lentivirus expressing a control shRNA (shCtrl) and shRNA against ANG (shANG) were cultured in hyperosmotic medium for 15 min, 30 min, 1 h, and 2 h, and cleavage of procaspases 3 and 9 was measured using Western blotting. As expected, the levels of both caspase 3 and 9 cleavage products during hyperosmotic stress were higher in shANG-

infected cells (Fig. 1F). In summary, our data showed that ANG reduces the rate of cell death in MEFs subjected to hyperosmotic stress. Next, we tested the molecular basis of this protective mechanism.

ANG inhibits apoptosis by attenuating Apaf-1 oligomerization and apoptosome activity. Hyperosmotic stress induces the intrinsic pathway of apoptosis, which involves as an initiating step the activation of procaspase 9 (25, 37). Activation of procaspase 9 requires interaction of released Cyt *c* with the cytoplasmic scaffolding protein Apaf-1 (4). Binding of Cyt *c* to Apaf-1 induces Apaf-1's conformational change and favors subsequent binding to dATP/ATP, thus allowing its oligomerization. The oligomerized Apaf-1 binds and cleaves procaspase 9 (1, 3). Because our data suggested that ANG delays the activation of procaspase 9 during hyperosmotic stress (Fig. 1A and B), we hypothesized that ANG attenuates Apaf-1 oligomerization and the downstream apoptosome formation, thus decreasing apoptosis.

To test our hypothesis we analyzed the effect of ANG on Apaf-1 oligomerization using gel filtration chromatography (Fig. 2). Extracts were prepared from untreated MEFs or cultured in hyperosmotic medium alone or in the presence of ANG. Equal amounts of protein were loaded on a Superose 6 column. In control extracts, Apaf-1 primarily localized with the lower-molecular-weight eluted fractions (monomeric Apaf-1), and procaspase 9 was not cleaved (Fig. 2A, top panel). As expected, in extracts cultured in hyperosmotic medium for 2 h, a considerable portion of the Apaf-1 protein moved to the heavy fractions due to its oligomerization and becoming part of the apoptosome (~700 kDa) (Fig. 2A, middle panel). Procaspase 9 in these extracts was significantly cleaved. In contrast, in extracts from cells cultured in hyperosmotic medium in the presence of ANG, Apaf-1 showed less association with the high-molecular-weight eluted fractions, suggesting a decrease in caspase 9 activation (Fig. 2A, bottom panel). In agreement with decreased apoptosome formation, a parallel decrease in the cleavage of procaspase 9 was also observed.

Because the experimental approach of determining Apaf-1 oligomerization via the use of gel filtration (Fig. 2A) is not quantitative, we also evaluated the caspase 9 activity in cells cultured in hyperosmotic medium alone or in the presence of ANG. ANG treatment caused a significant decrease in caspase 9 activity (Fig. 2B). However, caspase 3 activity showed a more significant decrease (Fig. 1C) than caspase 9 activity (Fig. 2B), suggesting that ANG inhibits apoptosome-mediated caspase 3 activity. To further support the idea that hyperosmotic stress induces caspase 3 activity via Apaf-1-mediated apoptosome formation, we compared hyperosmotic stress-induced caspase 3 cleavage between Apaf-$1^{+/+}$ and Apaf-$1^{-/-}$ MEFs (38). Both cell types responded to hyperosmotic stress by increasing the phosphorylation of α subunit of eukaryotic initiation factor 2 (eIF2α) (Fig. 2C), a signaling pathway that we have previously shown to lead to apoptosis in response to hyperosmotic stress (25). In agreement with our hypothesis, we did not observe caspase 3 cleavage in Apaf-$1^{-/-}$ MEFs (Fig. 2C).

Altogether, these data suggest that the antiapoptotic property of ANG agrees with the inhibition of intrinsic apoptotic pathway. Release of Cyt *c* from the mitochondria is the first signaling event associated with the intrinsic pathway (1, 3). We hypothesized that ANG-induced tiRNAs (Fig. 1D) can form complexes with cytoplasmic Cyt *c* and reduce formation or activity of the apoptosome (Fig. 1D). Thus, our studies suggest that ANG indirectly contributes to inhibition of apoptosome-mediated apoptosis.

Cytochrome *c* forms novel RNP complexes with ANG-induced tiRNAs during hyperosmotic stress. We recently reported that during hyperosmotic stress, MEFs undergo ANG-induced tRNA cleavage early in the stress response (20). Because the percentage of cleaved tRNAs was very low (18, 20, 21), MEFs were treated with exogenous ANG (0.5 μg/ml) during hyperosmotic stress in order to increase the accumulation of tiRNAs (Fig. 1D). We previously determined that a limiting factor for the generation of tiRNAs is tRNA substrate availability due to the absence of free tRNAs in the cytoplasm of cells (20); treatment of cells with increasing concentrations of ANG did not result in increased tiRNA accumulation (data not shown).

We hypothesized that the ANG-induced tiRNAs bind Cyt *c* during hyperosmotic stress and that this causes inhibition of apoptosome formation. To test our hypothesis, we performed immunoprecipitations (IP) for Cyt *c* from MEF cell lysates, either control (no stress) or cultured in hyperosmotic medium, for 15 min and 2 h. The treatments were performed in either the presence or the absence of ANG and did not affect the levels of Cyt *c* (Fig. 3A). Total RNA was isolated from the immunoprecipitates (IPs), 5′ end labeled with [γ-^{32}P]ATP, and run on denaturing polyacrylamide gels (Fig. 3B). The labeled full-length tRNA was observed in control as well as in stressed cells, indicating that the interaction between Cyt *c* and tRNAs is neither stress specific nor ANG treatment mediated (Fig. 3B). The labeling of full-length tRNA was lower in ANG-treated samples (Fig. 3B), suggesting a decreased affinity for binding of Cyt *c* to full-length tRNAs under ANG treatment (compare Fig. 1D and 3B). In the samples under hyperosmotic stress and treated for 2 h with ANG, in addition to the full-length labeled tRNAs, we observed strong labeling with a band of ~30 to 45 nt in size (Fig. 3B). This band migrated at a similar position with the tiRNAs in PAGE gels (Fig. 1D). The intensity of the RNA band corresponding to tiRNAs was much stronger than that of the full-length tRNA band at the 2-h time point (Fig. 3B). We have previously demonstrated that the highest total signal for tRNA cleavage in MEFs cultured in hyperosmotic medium occurred at 15 min, with a gradual decline thereafter (20). Because we did not observe an RNA band at the position that tiRNAs migrate in the Cyt *c*-immunoprecipitated samples from MEFs treated with hypertonic medium for 15 min, we propose that the binding of Cyt *c* to tiRNAs occurs after the release of Cyt *c* to the cytoplasm. These data do not exclude binding of low levels of released Cyt *c* to tiRNAs at earlier time points. However, because Cyt *c* has been reported to be released from mitochondria in a single step during apoptosis (39), it is unlikely that the earlier binding occurs.

In order to confirm that accumulation of tiRNAs is mainly a cytoplasmic phenomenon and does not occur in the mitochondria, we tested mitochondrial cell lysates for tiRNA accumulation during stress. We isolated mitochondria from MEFs incubated in hyperosmotic medium in the presence of ANG (Fig. 3C). Mitochondrial RNA and total RNA were 5′ end labeled with [γ-^{32}P]ATP and run on denaturing polyacrylamide gels. We did not observe any bands corresponding to tiRNAs in the mitochondrial RNA samples (Fig. 4D). These data support our hypothesis that during hyperosmotic stress the released Cyt *c* preferentially binds tiRNAs in the cytoplasm. Furthermore, exogenously added ANG during hyperosmotic stress increased the accumulation of tiRNAs

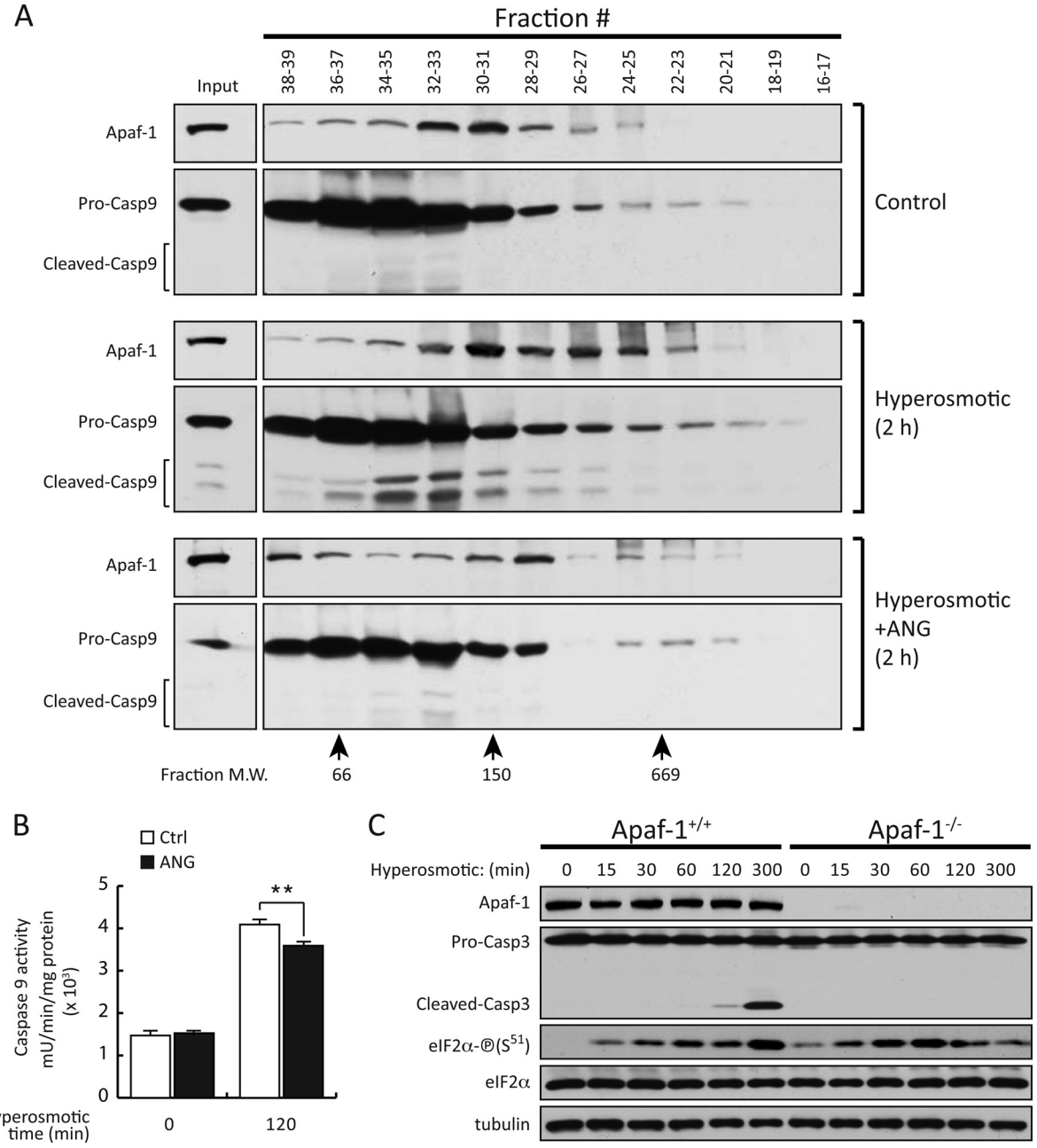

FIG 2 ANG inhibits apoptosis by decreasing Apaf-1 oligomerization and apoptosome activity. (A) MEFs were treated with normal medium (Control), hyperosmotic medium, or hyperosmotic medium in the presence of ANG (0.5 μg/ml) for 2 h. Total cell lysates were fractionated on a Superose 6 gel filtration column. Proteins isolated from the fractions were analyzed by Western blotting for the indicated proteins. The positions of molecular weight standards that were used for calibration of the column are marked at the bottom (arrows). (B) Caspase 9 activity in cell extracts from three biological replicates of MEFs treated with ANG for the indicated times. Error bars represent standard errors of three independent replicates (**, $P < 0.01$). (C) Western blot analysis of cell extracts from Apaf-$1^{+/+}$ and Apaf-$1^{-/-}$ MEFs incubated in hyperosmotic medium for the indicated proteins and the indicated times. P, phospho; M.W., molecular weight (in thousands).

at the time of increased cytoplasmic Cyt *c* accumulation and thus promoted their interaction.

Next-generation sequencing of RNAs (30 to 45 nt) derived from Cyt *c* IPs shows enrichment for a selected group of tiRNAs. RNA extracted from Cyt *c*-immunoprecipitated (Cyt *c*-IP) cell extracts isolated from cells incubated in hyperosmotic medium and ANG showed a much higher immunoprecipitation of small RNAs (similar in size to tiRNAs) than full-length tRNA (Fig. 3B). This suggests that Cyt *c* preferentially forms RNPs with RNAs of 30 to 45 nt in length, including tiRNAs. To uncover the population of ANG-generated tiRNAs that are preferentially bound to Cyt *c* upon hyperosmotic stress, we extracted total lysates from MEFs treated with ANG in hyperosmotic medium. The lysates were then split into two parts (Fig. 4A): one part served as the

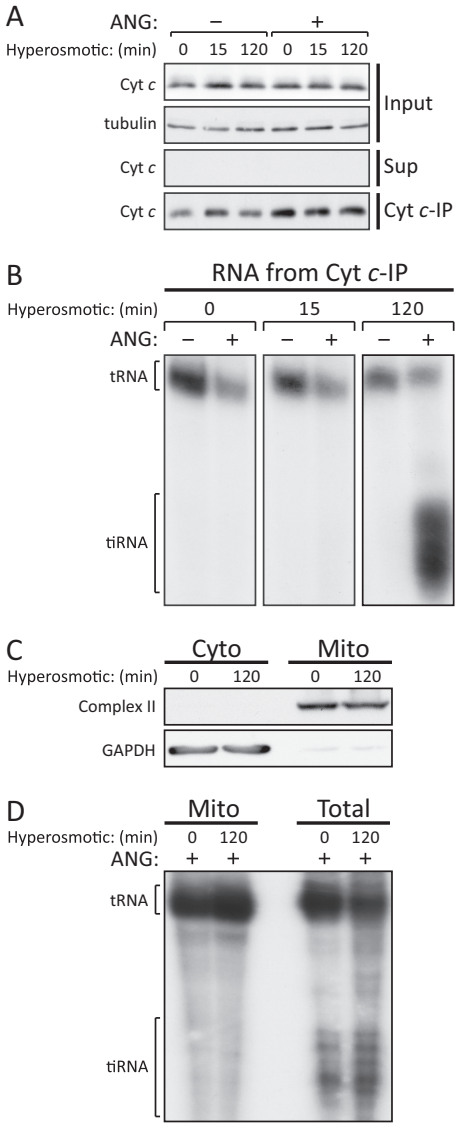

FIG 3 Cyt *c* forms complexes with ANG-induced tiRNAs during hyperosmotic stress. MEFs were incubated in hyperosmotic medium alone or in the presence of ANG (0.5 μg/ml) for the indicated times. (A) Total cell lysates were immunoprecipitated with a Cyt *c* antibody. The inputs, supernatants (Sup), and immunoprecipitates (Cyt *c*-IP) were analyzed by Western blotting for the indicated proteins. (B) RNA was isolated from the Cyt *c*-IPs, 5′ [γ-^{32}P]ATP end labeled, and analyzed as described in the legend of Fig. 1D. (C) Mitochondrial (Mito) and cytosolic (Cyto) extracts were analyzed by Western blotting for the indicated proteins. (D) RNA isolated from the mitochondrial lysates was 5′ [γ-^{32}P]ATP end labeled and analyzed as described in the legend of Fig. 1D. The migrations of tRNAs and tiRNAs are indicated with brackets.

control (Fig. 4A, Ctrl), consisting of the RNA content of the lysates, and the second part was the Cyt *c*-immunoprecipitated fraction, consisting of the RNA content that is bound to Cyt *c* (Cyt *c*-IP). Both fractions were separated using PAGE and selected for small RNAs of ~30 to 45 nucleotides, in triplicates, and sent to next-generation sequencing. Analysis of the sequencing data should determine the enrichment of the tiRNAs species in the Cyt *c*-immunoprecipitated RNA by normalizing data from high-throughput sequencing of RNA transcripts (RNA-seq) from the IP/control lysates. This experimental approach would also allow the identification of factors that may play a role in the binding of Cyt *c* to tiRNAs, such as sequence, structure, etc.

The deep-sequencing data were mapped on the *Mus musculus* genome (mm10 version). For the control, about 71% of 67 million reads were mapped, while 85% of 2.5 million reads were mapped for the for Cyt *c*-IP. The quality of the deep-sequencing data was assessed by the reproducibility of RNA gene expression levels in two out of three biological replicates for both the control (R^2 = 0.97) and the Cyt *c*-IP (R^2 = 0.98) fractions (Fig. 4B).

Preferentially bound RNA fragments to Cyt *c* would show enrichment in the IP fraction compared to the control fraction. To compute the enrichment of a gene, we first started by collecting all deep-sequencing reads mapping to it, thus assembling its mountain plot. Because we have two deep-sequencing sets or fractions (control and IP), each gene has two mountain plots (Fig. 4C and Fig. 5) that are directly comparable, once normalized by the total number of mapped reads (which accounts for the deep-sequencing depth which may differ between deep-sequencing runs). The enrichment is defined as the $\log_2$ ratio of heights where the IP and control curves are the most distant from one another. Selected mountain plots for tiRNAs are shown in Fig. 4C and Fig. 5 as most enriched mountains have a width of about ~35 nt and have a strong 5′ or 3′ bias. All mountain plots showed a valley between nucleotide positions 30 and 40 of tRNAs, where ANG is expected to cut and which would correspond to the apex of the anticodon loop. If we compare tRNAs from the cytoplasm- and mitochondrion-encoded tRNAs, we observe that cytoplasmic tRNAs are far more preferred by Cyt *c* after hyperosmotic stress and ANG treatment (Fig. 4D). A list of tiRNAs with enrichment values greater than 4 is shown in Fig. 4E.

We should emphasize that the computation of the enrichment is performed to uncover the tRNA isoacceptors whose abundance in the Cyt *c*-RNP complex is greater than the total cell-wide abundance of isoacceptors (as a control). Because these two conditions yield different amounts of total tRNAs, we can normalize the deep-sequencing counts of a given isoacceptor under a given condition by the rpkM (reads per kilobase per million mapped) of that condition. From there, we do not compare the relative abundance of the various isoacceptors within a given condition, but, rather, we compare the abundance of the same isoacceptor between two different conditions. In that way, the relative abundance of the tRNA isoacceptors *in vivo* is not a factor for adjustment. In all, if there were no differences between the two conditions, the subsequent enrichment computation for a given isoacceptor between the two conditions would result in a value close to 0 (i.e., $\log_2$ 1) even if the two conditions had made for discordant total tRNA quantities.

Cyt *c* binds tiRNAs *in vitro*. It has been shown that Cyt *c* binds full-length *in vitro*-synthesized tRNAs (cytoplasm and mitochondrion encoded) with higher affinity than other RNAs, such as mRNAs and rRNAs (29). We have shown here that Cyt *c* bound tiRNAs *in vivo* at the time that it was released from the mitochondria during hyperosmotic stress. In addition, we showed enrichment for a small group of tiRNAs in complexes with Cyt *c* (Fig. 4E).

We next determined *in vitro* the affinity ($K_{1/2}$) of Cyt *c* for a selected group of individual tiRNAs, for full-length tRNA^{Met}, and for the tiRNA-containing RNA pool (tiRNA^{*pool}) that was immunoprecipitated with Cyt *c* (Fig. 6). Individual tiRNAs and tRNA^{Met} were synthetically produced and radiolabeled. The tiRNA^{*pool}

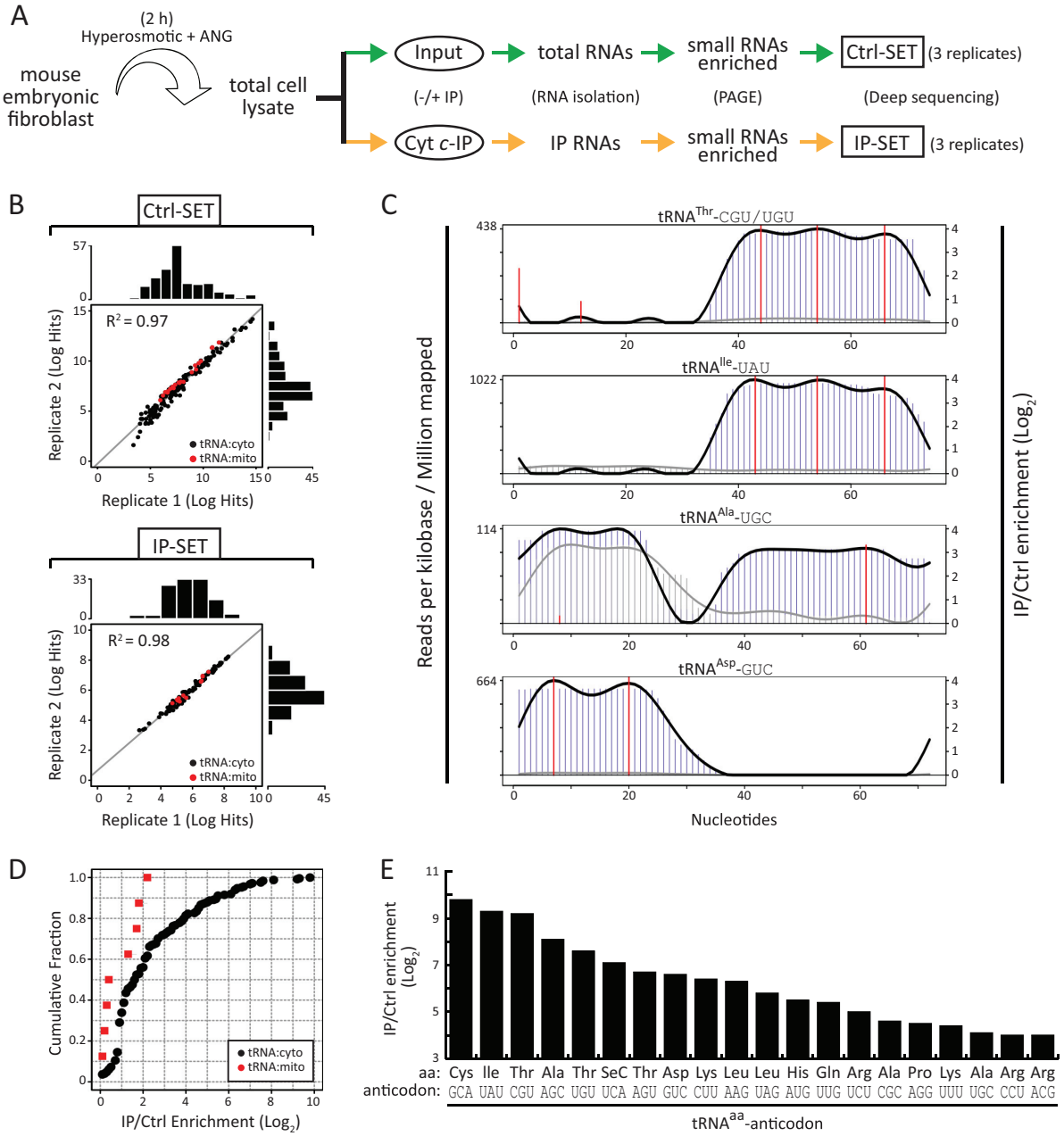

FIG 4 Next-generation sequencing of RNAs immunoprecipitated with Cyt *c* shows enrichments for some tiRNAs. (A) Experimental scheme of the RNA-seq experiment for the detection of tiRNAs accumulated in Cyt *c*-IPs versus tiRNAs in total cell lysates during hyperosmotic stress in the presence of ANG. The two experimental tracks, control (Ctrl-SET, green) and Cyt *c*-IP (IP-SET, yellow), were performed in triplicates, and samples enriched in small RNAs were sent to deep sequencing after a PAGE gel purification. (B) Correlation plots between two replicates of deep-sequencing data mapping on tRNA genes: control and Cyt *c*-IP enriched. Each dot represents a tRNA gene; red dots represent mitochondrial tRNA genes. (C) Enrichment plots for selected tRNA genes. Each plot shows the deep-sequencing reads mapped along the tRNA gene for both the control (gray line) and Cyt *c*-IP-enriched (black line) data sets. Values on *y* axes are in reads per kilobase per million mapped (rpkM), allowing a direct comparison of the data. Enriched regions are shown with vertical red bars. (D) Cumulative fractions of various small tRNA species as a function of enrichment. (E) Distribution of Cyt *c*-IP enrichment values for tRNA genes. For clarity, only genes with an enrichment value greater than 4 are shown. Enrichment plots for tRNAs in panel E are shown in Fig. 5. aa, amino acid.

bound at a low micromolar concentration to Cyt *c* (Fig. 6A and B). Full-length $tRNA^{Met}$ bound with slightly lower affinity than the immunoprecipitated $tiRNA^{*pool}$ (Fig. 6C). Affinities of Cyt *c* for different tiRNAs varied considerably, ranging from a $K_{1/2}$ of 26.9 ± 6.8 μM for $tiRNA^{Arg}$ to a $K_{1/2}$ of 190.4 ± 13.8 μM for $tiRNA^{Ala}$ (Fig. 6B and C). However, there was little correlation between affinities *in vitro* and enrichment of the tiRNA fragments *in vivo*. These data suggest that the affinity of Cyt *c* for unmodified tiRNAs is unlikely to drive the observed enrichment of the tiRNAs *in vivo* (Fig. 4). The significantly higher affinity of the $tiRNA^{*pool}$ than the individual synthetic tiRNAs suggests that in cells the selectivity of Cyt *c* for a subset of tiRNAs is influenced by tRNA

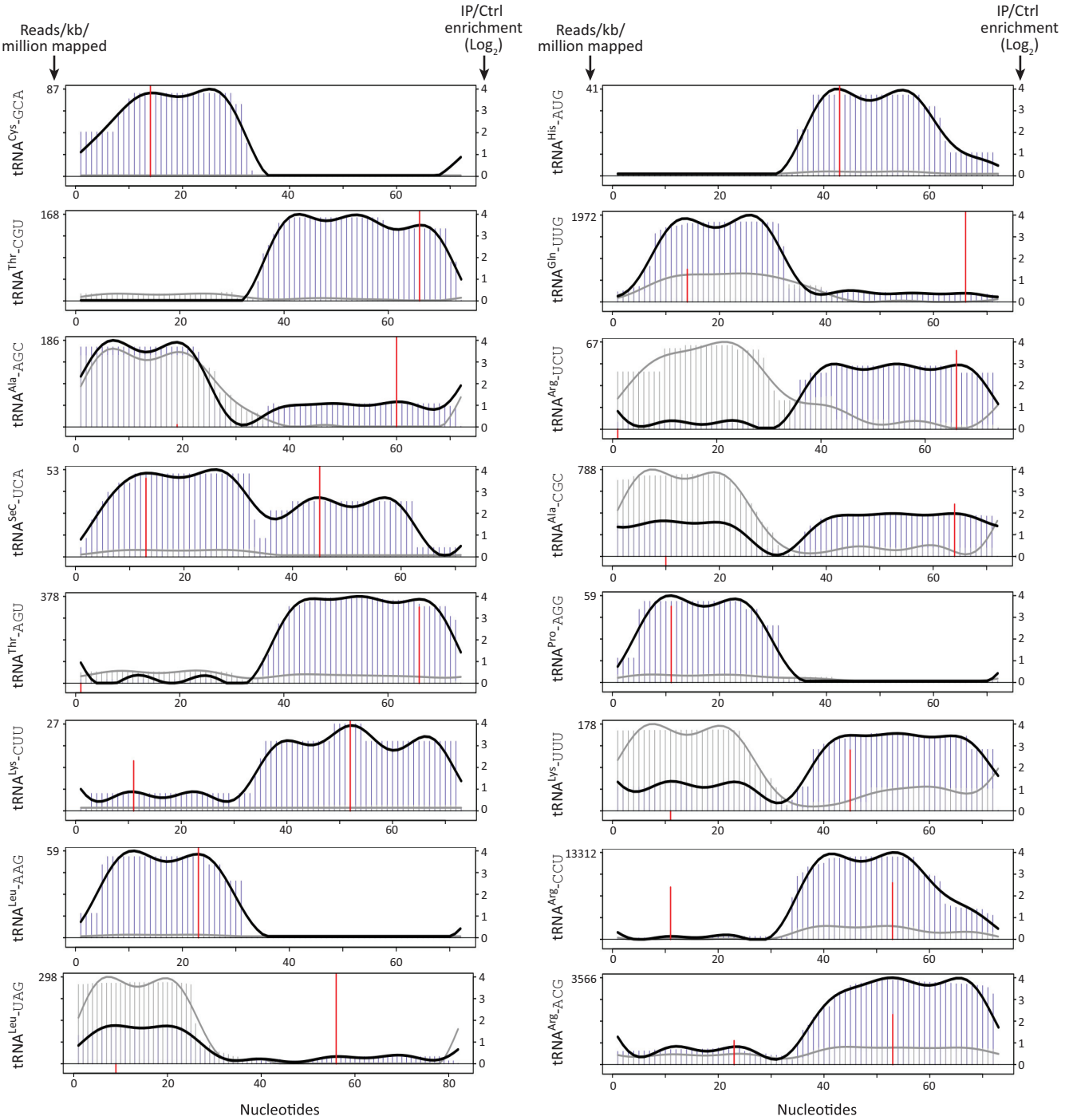

FIG 5 Enrichment plots for selected tRNA genes. Each plot shows the deep-sequencing reads mapped along the tRNA gene for both the control (gray line) and Cyt *c*-IP-enriched (black line) data sets. Values on *y* axes are in reads per kilobase per million mapped (rpkM), allowing a direct comparison of the data. Enriched regions are shown with vertical red bars and correspond to IP peaks. The enrichment of a given tRNA is the maximum enrichment value among all enriched peaks. The enrichment value at a peak is the $\log_2$ ratio of the height of the IP curve to the height of the control curve evaluated at the position of the peak of the IP curve.

modifications (40), other cellular factors, or both. Although there are over 100 posttranscriptional modifications of tiRNAs, the biological significance of most modifications is not known (41, 42).

As a final test of the specificity of binding of Cyt *c* to tiRNAs compared to tRNAs, we used gel mobility shift assays in which the migration of the RNA and RNA-protein complexes was visualized by methylene blue staining (32). We first showed that tiRNA^{Arg} and Cyt *c* form high-molecular-weight complexes by incubating tiRNA^{Arg} with increasing concentrations of Cyt *c* (Fig. 6D). The addition of tRNA in increasing concentrations in the binding as-

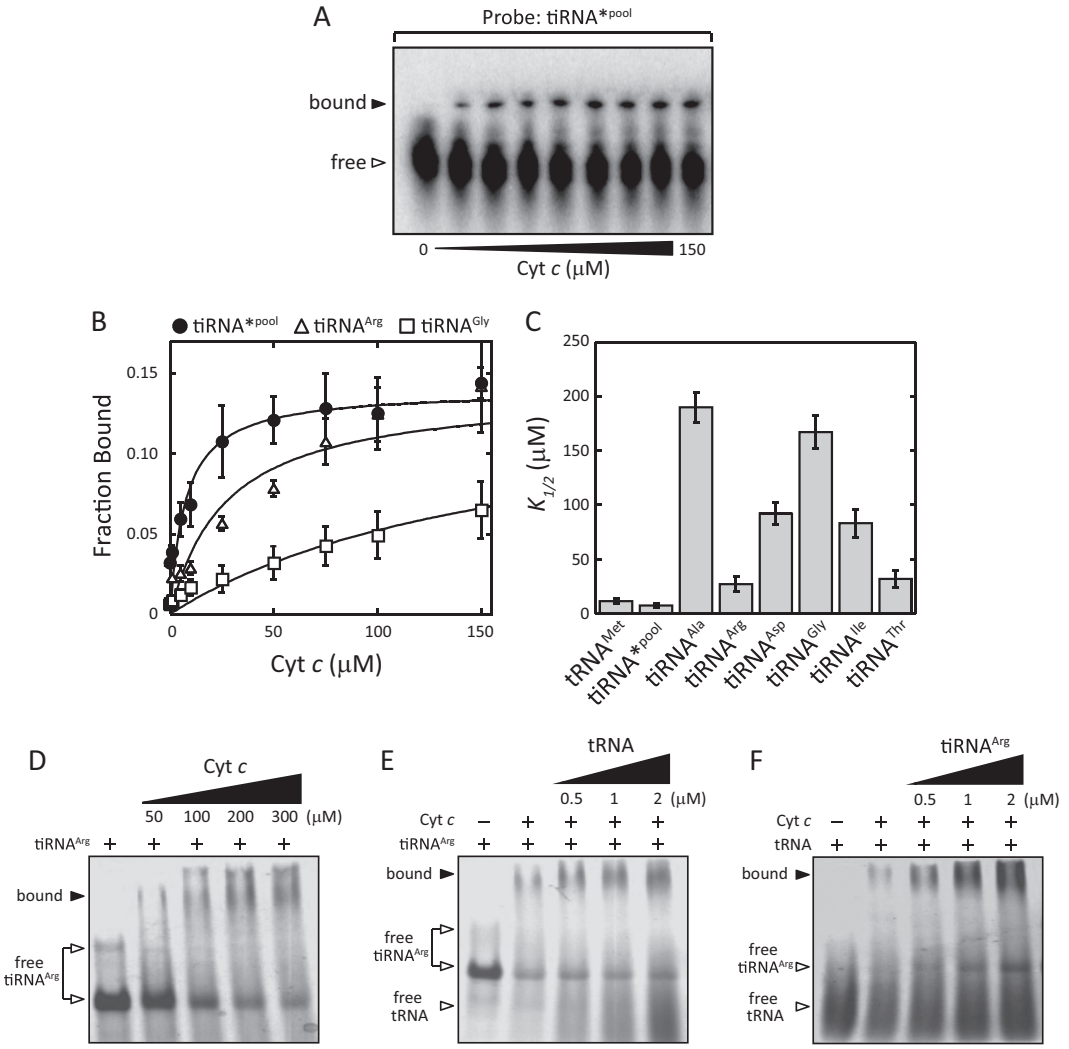

FIG 6 Cyt *c* binds tiRNAs *in vitro*. (A) Cyt *c* binding was measured by gel mobility shift assays. Representative gel for the tiRNA^{*pool} is shown. The tiRNA^{*pool} is the same material that was sent for next-generation sequencing in the IP-SET (Fig. 4A). The asterisk indicates that tiRNAs are not the only components of the tiRNA pool. (B) Binding isothermes for tiRNA^{*pool}, tiRNA^{Arg}, and tiRNA^{Gly}. Error bars represent standard errors of three independent experiments. (C) Apparent affinities ($K_{1/2}$) were calculated for the full-length tRNA^{Met}, the tiRNA^{*pool}, and the indicated tiRNA species. Error bars represent standard errors of three independent experiments. (D) Electrophoretic mobility shift assay of RNA binding reaction mixtures containing tiRNA^{Arg} (1 μM) and the indicated concentrations of Cyt *c*. (E) Electrophoretic mobility shift assay of RNA-binding reaction mixtures containing Cyt *c* (100 μM), tiRNA^{Arg} (1 μM), and the indicated concentrations of total yeast tRNA. (F) Electrophoretic mobility shift assay of RNA-binding reaction mixtures containing Cyt *c* (100 μM), total yeast tRNA (1 μM), and the indicated concentrations of tiRNA^{Arg}. Empty triangles denote free RNA of either yeast tRNA or tiRNA^{Arg}. Solid triangles indicate bound complex from Cyt *c* and RNA.

says of tiRNA^{Arg} with Cyt *c* did not compete binding of Cyt *c* to tiRNA^{Arg} (Fig. 6E). Instead, it caused the formation of higher-intensity complexes of Cyt *c* with RNA (Fig. 6E). These data suggest that both tRNA and tiRNA^{Arg} form complexes with Cyt *c* and that tiRNA^{Arg} competes well with the tRNA for binding to Cyt *c*. The latter was further supported by the gel mobility shift assay of tRNA with Cyt *c* in the presence of increasing concentrations of tiRNA^{Arg} (Fig. 6F). The addition of tiRNA^{Arg} led to increased high-molecular-weight complex formation, further supporting the idea that both tRNA and tiRNA^{Arg} form complexes with Cyt *c* (Fig. 6E and F).

ANG protects primary neurons from hyperosmotic stress-induced apoptosis. We used primary cortical neurons as a model to demonstrate the therapeutic potential of ANG on neuronal cell viability during hyperosmotic stress. We tested whether induction of apoptosis by hyperosmotic stress is decreased by the addition of ANG into cortical neurons. Cortical neurons were generated from 1- to 2-day-old mouse embryos (25). Exposure of neurons to hyperosmotic stress induced apoptosis (Fig. 7A). However, the addition of ANG in the hyperosmotic medium was neuroprotective. Quantification by TUNEL staining showed that 62% of neurons cultured in hyperosmotic medium alone were TUNEL positive, compared to 33% TUNEL-positive neurons of those exposed to hyperosmotic stress in the presence of ANG for 2 h (Fig. 7A). In addition, ANG treatment during hyperosmotic stress also decreased the cleavage of procaspase 9 (Fig. 7B). In a similar manner, ANG-mediated protection was observed by performing a cell survival assay (Fig. 7C). Taken together, these facts suggest that the

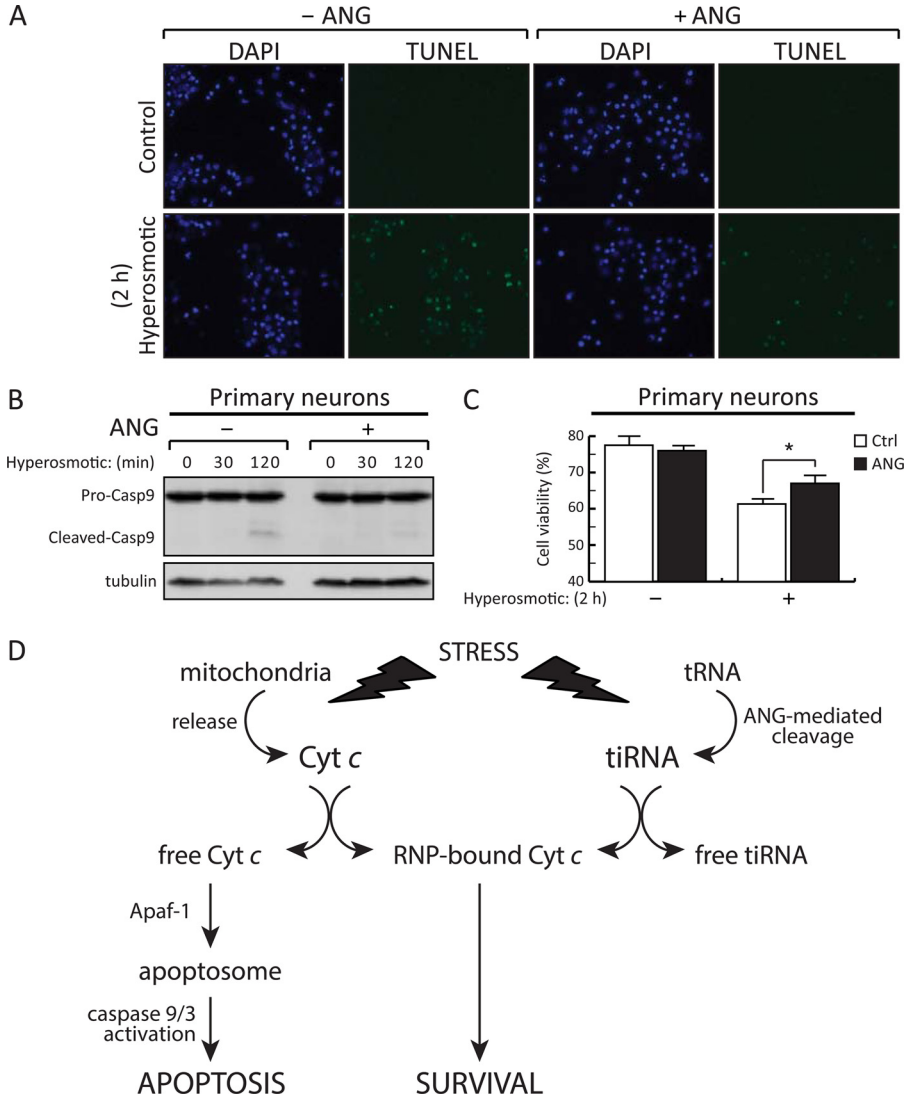

FIG 7 ANG protects primary neurons from hyperosmotic stress-induced apoptosis. Primary cortical neurons from C57BL/6J pups, cultured for 7 days and incubated for 2 h in either hyperosmotic medium alone or in the presence of ANG, were used for TUNEL staining (representative image) (A), Western blotting of total cell lysates for the indicated proteins (B), and cell viability measured by the Muse cell count instrument (C). Error bars represent standard errors of three independent replicates (*, $P < 0.05$). (D) Schematic representation of ANG-induced tiRNA-mediated regulation of apoptosome formation during hyperosmotic stress. It is shown that ANG (exogenous or activated by stress) generates tiRNAs by cleavage of tRNAs. Cyt *c* released from mitochondria forms complexes with the tiRNAs within a not fully characterized RNA-protein complex (RNP, ribonucleoprotein complex). Sequestration of Cyt *c* in the tiRNA-containing RNPs either limits its availability for association with Apaf-1, thus decreasing apoptosome formation, or inhibits apoptosome activity and induction of apoptosis.

addition of ANG into cortical neurons during hyperosmotic stress accompanies decreased apoptosis. The findings also highlight the potential importance of ANG in neuronal cell survival under different stresses or pathological conditions.

DISCUSSION

Hyperosmotic stress is known to induce the intrinsic pathway of apoptosis (25) that involves Cyt *c* release from the mitochondria and subsequent apoptosome formation and activation of the caspases. However, mitochondrial dysfunction does not always result in Cyt *c* release (2, 43). It is the association of Cyt *c* with Apaf-1 in the cytoplasm that causes the activation of caspases, leading to apoptotic degradation of cellular components. However, there might be pathways that could prevent Cyt *c* association with Apaf-1, thus making the release of Cyt *c* "harmless" for induction of apoptosis (43). In this report we have identified and characterized a mechanism that inhibits Cyt *c*/Apaf-1-mediated activation of the apoptosome in cells subjected to hyperosmotic stress. We found that Cyt *c* released from the mitochondria during hyperosmotic stress forms RNPs with small RNAs that include tiRNAs generated by the actions of ANG. This association was correlated with decreased formation and activity of the apoptosome that involves Apaf-1–Cyt *c* binding and caspase 9 cleavage. Our studies reveal (i) a novel signaling pathway that interferes with Cyt *c*-mediated caspase activation, (ii) a novel function of tiRNAs as inhibitors of apoptosome formation and function, and (iii) a novel antiapoptotic mechanism involving ANG-mediated tRNA cleavage.

Cleavage of tRNAs is conserved among eukaryotes, specifically in response to oxidative stress by secreted ribonucleases (RNY1 in yeast [23] and ANG in mammalian cells [18]). In almost all cases of stress-induced tRNA cleavage, the cleavage site was suggested to be at or close to the anticodon loop (16). The functional significance of the produced tiRNAs is not clear. It has been suggested that tiRNAs could target specific signaling pathways, potentially modulating the cellular response to stress (16). For example, tiRNAs may play a role in the inhibition of translation initiation during stress via interaction with the translational silencer YB1 and sequestration of mRNAs in stress granules (44). Interestingly, optimal inhibition of translation and stress granule formation were induced by 5′ tiRNAs but not by 3′ tiRNAs (21, 27, 44). This is in contrast to our findings here that both 5′ and 3′ tiRNAs are selectively enriched in the novel Cyt *c*-RNP complex. More recently, it was shown that oxidative stress induced by arsenite treatment of HeLa cells inhibited translation elongation concomitant with ANG-mediated cleavage of the aminoacyl-ends of all tRNAs (45). This observation may explain the decreased association of Cyt *c* with full-length tRNAs during ANG treatment (Fig. 3B). Taken together, these previous studies presented a connection between the inhibition of translation in stressed cells and the ANG-mediated cleavage of tRNAs.

Our studies describe a new function of tiRNAs in the formation of complexes with Cyt *c* in the cytoplasm of stressed cells. It is noteworthy that Cyt *c* complex formation with tiRNAs occurred at the time that Cyt *c* was released from the mitochondria into the cytoplasm (Fig. 3B), further suggesting that these complexes are the result of specific binding of tiRNAs with Cyt *c* in the cell. The specificity of complex formation of Cyt *c* with tiRNAs was further challenged by the low levels of Cyt *c* coimmunoprecipitated with full-length tRNAs, which are in high abundance relative to tiRNAs (Fig. 3B). We have previously shown that tRNAs, and not tiRNAs, are in complexes with eIF2 and eEF1A in cells treated with ANG during hyperosmotic stress (20). That observation suggested that tRNAs bound by translation factors are not prone to cleavage by ANG (20). It is therefore logical to suggest that Cyt *c* released in the cytoplasm during hyperosmotic stress forms complexes enriched in tiRNAs and not tRNAs due to the low availability of free full-length tRNAs. A schematic representation of the actions of the Cyt *c*-RNP complex in inhibition of apoptosome formation during osmotic stress is given in Fig. 7D.

Prior reports (29, 30) and our finding here (Fig. 3B and 6) support that the idea full-length tRNA can bind Cyt *c in vivo* and *in vitro*. It has also been reported that binding of full-length tRNA to Cyt *c* can inhibit apoptosome formation *in vitro* (29). Moreover, treatment of cells with onconase, which cleaves tRNA (46), induced caspase 9 cleavage and apoptosis, further supporting the idea that full-length tRNA integrity protects healthy cells from apoptosis. Similar to the functions of full-length tRNA in healthy cells, tiRNA complexed with Cyt *c* during stress is concurrent with the inhibition of caspase 9 cleavage and apoptosome formation (Fig. 2). Enrichment for specific tRNA isoacceptors/isodecoders was observed in the Cyt *c*-tiRNA complex (Fig. 4). The molecular mechanism for this enrichment is not known yet and is beyond the scope of this work. The *in vitro* binding experiments of Cyt *c* to chemically synthesized tiRNAs (Fig. 6C) did not show a good correlation with the enrichment plot (Fig. 4E). For example, tiRNA^{Ala}-AGC (where AGC is the anticodon) showed lower affinity than tiRNA^{Arg}-ACG although enrichment values were similar (Fig. 4 and 6). Moreover, *in vitro* binding assays of Cyt *c* to the tiRNA^{*pool} revealed that the affinity of binding for the tiRNA^{*pool} was better than that of tiRNA^{Arg}-ACG and tRNA^{Met} (Fig. 6C). Because we showed that at least tiRNA^{Arg}-ACG binds Cyt *c in vitro* with comparable affinity to that of the full-length tRNA^{Met} (Fig. 6C), we can speculate that the tertiary structure of specific tiRNAs may determine the specificity of binding. Interaction of Cyt *c* with tiRNAs *in vivo* may include additional factors that assist folding of the tiRNAs, thus contributing to the enrichment of specific tiRNAs in the Cyt *c* complex. Such factors can be other proteins or small RNAs, as well as posttranscriptional modifications of the tRNAs themselves. The inability of *in vitro*-synthesized tRNAs or tiRNAs to form stable structures that can bind Cyt *c* with high affinity may be due to the lack of modifications.

Posttranscriptional modification of tRNAs is a highly conserved phenomenon (47) and is an important factor for their folding and integrity *in vivo* (42). The modification status of tiRNAs might be one of the factors that determine the structure and binding affinities of these molecules to their interacting partners, i.e., more specifically to Cyt *c*. Very few reports in the literature describe the modification status of tRNAs *in vivo*, especially in mammalian tRNAs. The tRNA modification N^1-methyl-adenosine (m1A58) at the conserved nucleotide 58 in the TΨC loop is present in most eukaryotic tRNAs (48). The only account describing the m1A58 modification levels in human tRNAs showed that this modification can occur in unknown fractions of many tRNAs. In HeLa cells, 9 out of the 40 tRNAs tested were found to be hypomodified (46). We examined the enrichment plot of these nine tRNAs to see if there was any correlation between the hypomodification status of the A58 nucleotide and Cyt *c*-IP enrichment on the 3′ end of the tRNAs. The enrichment plots of these tRNAs did not show a preference for 3′ enrichment. Some tRNAs (tRNA^{Pro}-hGG, tRNA^{Glu}-yUC, tRNA^{His}-GUG, and tRNA^{Trp}-CCA) did not show enrichment on either fragment, three (tRNA^{Ala}-AGC, tRNA^{Leu}-CAA, and tRNA^{Val}-UAC) showed enrichment on the 3′ fragment, and two (tRNA^{Asp}-GUC and tRNA^{Leu}-UAA) showed 5′ enrichment. These data led us to believe that the effect of the m1A58 modification, although possible, does not significantly affect the enrichment of tiRNAs in the Cyt *c*-RNP.

Several studies show that ANG protects motor neuron degeneration induced by various stresses, including excitotoxicity, endoplasmic reticulum stress, and hypoxia (12–14). Our studies also showed that addition of ANG inhibits hyperosmotic stress-induced apoptosis in primary neurons (Fig. 7). Although the cytoprotective effects of ANG may involve signaling pathways other than its nuclease activity on tRNAs (16, 49–51), our data strongly suggest that ANG inhibits the intrinsic pathway of apoptosis during hyperosmotic stress due to complex formation of Cyt *c* with tiRNAs. So, in addition to other cytoprotective actions of ANG, the inhibition of the apoptosome may be unique via the presence of tiRNAs. The investigation of the mechanism of tiRNA-mediated inhibition of apoptosome formation and activity is an interesting future direction in a challenging field (52–54).

Inhibition of the apoptosome via ANG-mediated Cyt *c* tiRNA complex formation can be used as a valuable therapeutic strategy. Although our current studies did not determine the exact tiRNA structures that bind Cyt *c*, they do provide a pool of specific tiRNA molecules with potential cytoprotective properties in response to stress. RNA-based therapeutics is an emerging field. Future studies leading to the discovery of all the components of the tiRNA-

apoptosome inhibitory complex will shed light on the molecular mechanisms that drive formation of these complexes during stress and protect cells from the deleterious effects of Cyt *c*–Apaf-1 association and activation of apoptosis.

ACKNOWLEDGMENTS

This work was supported, in whole or in part, by grants R37-DK060596 and R01-DK053307 (to M.H.) and by grants R01-GM067720 and R01-GM099720 (E.J.) from the National Institutes of Health. N.B.V.S. was supported by funds from DBT-India, a DST-FIST grant to the Department of Biochemistry, University of Hyderabad. M.G. was supported by a Senior Research Fellowship from CSIR, India. M.P. was a Chicago Fellow of the University of Chicago and is a Natural Sciences and Engineering Research Council of Canada postdoctoral fellow.

We thank Jing Wu and Scott A. Becka, Case Western Reserve University, for technical assistance. Apaf-$1^{+/+}$ and Apaf-$1^{-/-}$ MEFs were a generous gift from Tak W. Mak (Ontario Cancer Institute).

REFERENCES

1. **Tait SW, Green DR.** 2010. Mitochondria and cell death: outer membrane permeabilization and beyond. Nat. Rev. Mol. Cell Biol. **11:**621–632. http://dx.doi.org/10.1038/nrm2952.
2. **Li P, Nijhawan D, Wang X.** 2004. Mitochondrial activation of apoptosis. Cell **116:**S57–S59. http://dx.doi.org/10.1016/S0092-8674(04)00031-5.
3. **Reubold TF, Eschenburg S.** 2012. A molecular view on signal transduction by the apoptosome. Cell Signal. **24:**1420–1425. http://dx.doi.org/10.1016/j.cellsig.2012.03.007.
4. **Zou H, Li Y, Liu X, Wang X.** 1999. An APAF-1.cytochrome *c* multimeric complex is a functional apoptosome that activates procaspase-9. J. Biol. Chem. **274:**11549–11556. http://dx.doi.org/10.1074/jbc.274.17.11549.
5. **Adams JM, Cory S.** 2002. Apoptosomes: engines for caspase activation. Curr. Opin. Cell Biol. **14:**715–720. http://dx.doi.org/10.1016/S0955-0674(02)00381-2.
6. **Jiang X, Wang X.** 2000. Cytochrome *c* promotes caspase-9 activation by inducing nucleotide binding to Apaf-1. J. Biol. Chem. **275:**31199–31203. http://dx.doi.org/10.1074/jbc.C000405200.
7. **Purring-Koch C, McLendon G.** 2000. Cytochrome *c* binding to Apaf-1: the effects of dATP and ionic strength. Proc. Natl. Acad. Sci. U. S. A. **97:**11928–11931. http://dx.doi.org/10.1073/pnas.220416197.
8. **Kurokawa M, Zhao C, Reya T, Kornbluth S.** 2008. Inhibition of apoptosome formation by suppression of Hsp90β phosphorylation in tyrosine kinase-induced leukemias. Mol. Cell. Biol. **28:**5494–5506. http://dx.doi.org/10.1128/MCB.00265-08.
9. **Pandey P, Saleh A, Nakazawa A, Kumar S, Srinivasula SM, Kumar V, Weichselbaum R, Nalin C, Alnemri ES, Kufe D, Kharbanda S.** 2000. Negative regulation of cytochrome c-mediated oligomerization of Apaf-1 and activation of procaspase-9 by heat shock protein 90. EMBO J. **19:**4310–4322. http://dx.doi.org/10.1093/emboj/19.16.4310.
10. **Favaloro B, Allocati N, Graziano V, Di Ilio C, De Laurenzi V.** 2012. Role of apoptosis in disease. Aging (Albany, NY) **4:**330–349.
11. **Iwasaki Y, Ikeda K, Kinoshita M.** 2002. Molecular and cellular mechanism of glutamate receptors in relation to amyotrophic lateral sclerosis. Curr. Drug Targets CNS Neurol. Disord. **1:**511–518. http://dx.doi.org/10.2174/1568007023339021.
12. **Kieran D, Sebastia J, Greenway MJ, King MA, Connaughton D, Concannon CG, Fenner B, Hardiman O, Prehn JH.** 2008. Control of motoneuron survival by angiogenin. J. Neurosci. **28:**14056–14061. http://dx.doi.org/10.1523/JNEUROSCI.3399-08.2008.
13. **Aparicio-Erriu IM, Prehn JH.** 2012. Molecular mechanisms in amyotrophic lateral sclerosis: the role of angiogenin, a secreted RNase. Front. Neurosci. **6:**167. http://dx.doi.org/10.3389/fnins.2012.00167.
14. **Thiyagarajan N, Ferguson R, Subramanian V, Acharya KR.** 2012. Structural and molecular insights into the mechanism of action of human angiogenin-ALS variants in neurons. Nat. Commun. **3:**1121. http://dx.doi.org/10.1038/ncomms2126.
15. **Acharya KR, Shapiro R, Allen SC, Riordan JF, Vallee BL.** 1994. Crystal structure of human angiogenin reveals the structural basis for its functional divergence from ribonuclease. Proc. Natl. Acad. Sci. U. S. A. **91:**2915–2919. http://dx.doi.org/10.1073/pnas.91.8.2915.
16. **Li S, Hu GF.** 2012. Emerging role of angiogenin in stress response and cell survival under adverse conditions. J. Cell Physiol. **227:**2822–2826. http://dx.doi.org/10.1002/jcp.23051.
17. **Tello-Montoliu A, Patel JV, Lip GY.** 2006. Angiogenin: a review of the pathophysiology and potential clinical applications. J. Thromb. Haemost. **4:**1864–1874. http://dx.doi.org/10.1111/j.1538-7836.2006.01995.x.
18. **Yamasaki S, Ivanov P, Hu GF, Anderson P.** 2009. Angiogenin cleaves tRNA and promotes stress-induced translational repression. J. Cell Biol. **185:**35–42. http://dx.doi.org/10.1083/jcb.200811106.
19. **Thompson DM, Parker R.** 2009. Stressing out over tRNA cleavage. Cell **138:**215–219. http://dx.doi.org/10.1016/j.cell.2009.07.001.
20. **Saikia M, Krokowski D, Guan BJ, Ivanov P, Parisien M, Hu GF, Anderson P, Pan T, Hatzoglou M.** 2012. Genome-wide identification and quantitative analysis of cleaved tRNA fragments induced by cellular stress. J. Biol. Chem. **287:**42708–42725. http://dx.doi.org/10.1074/jbc.M112.371799.
21. **Fu H, Feng J, Liu Q, Sun F, Tie Y, Zhu J, Xing R, Sun Z, Zheng X.** 2009. Stress induces tRNA cleavage by angiogenin in mammalian cells. FEBS Lett. **583:**437–442. http://dx.doi.org/10.1016/j.febslet.2008.12.043.
22. **Thompson DM, Lu C, Green PJ, Parker R.** 2008. tRNA cleavage is a conserved response to oxidative stress in eukaryotes. RNA **14:**2095–2103. http://dx.doi.org/10.1261/rna.1232808.
23. **Thompson DM, Parker R.** 2009. The RNase Rny1p cleaves tRNAs and promotes cell death during oxidative stress in Saccharomyces cerevisiae. J. Cell Biol. **185:**43–50. http://dx.doi.org/10.1083/jcb.200811119.
24. **Lee SR, Collins K.** 2005. Starvation-induced cleavage of the tRNA anticodon loop in Tetrahymena thermophila. J. Biol. Chem. **280:**42744–42749. http://dx.doi.org/10.1074/jbc.M510356200.
25. **Bevilacqua E, Wang X, Majumder M, Gaccioli F, Yuan CL, Wang C, Zhu X, Jordan LE, Scheuner D, Kaufman RJ, Koromilas AE, Snider MD, Holcik M, Hatzoglou M.** 2010. eIF2α phosphorylation tips the balance to apoptosis during osmotic stress. J. Biol. Chem. **285:**17098–17111. http://dx.doi.org/10.1074/jbc.M110.109439.
26. **Burg MB, Ferraris JD, Dmitrieva NI.** 2007. Cellular response to hyperosmotic stresses. Physiol. Rev. **87:**1441–1474. http://dx.doi.org/10.1152/physrev.00056.2006.
27. **Ivanov P, Emara MM, Villen J, Gygi SP, Anderson P.** 2011. Angiogenin-induced tRNA fragments inhibit translation initiation. Mol. Cell **43:**613–623. http://dx.doi.org/10.1016/j.molcel.2011.06.022.
28. **Mei Y, Stonestrom A, Hou YM, Yang X.** 2010. Apoptotic regulation and tRNA. Protein Cell **1:**795–801. http://dx.doi.org/10.1007/s13238-010-0107-x.
29. **Mei Y, Yong J, Liu H, Shi Y, Meinkoth J, Dreyfuss G, Yang X.** 2010. tRNA binds to cytochrome c and inhibits caspase activation. Mol. Cell **37:**668–678. http://dx.doi.org/10.1016/j.molcel.2010.01.023.
30. **Suryanarayana T, Uppala JK, Garapati UK.** 2012. Interaction of cytochrome *c* with tRNA and other polynucleotides. Mol. Biol. Rep. **39:**9187–9191. http://dx.doi.org/10.1007/s11033-012-1791-9.
31. **Chan PP, Lowe TM.** 2009. GtRNAdb: a database of transfer RNA genes detected in genomic sequence. Nucleic Acids Res. **37:**D93–D97. http://dx.doi.org/10.1093/nar/gkn787.
32. **Gorla M, Sepuri NB.** 2014. Perturbation of apoptosis upon binding of tRNA to the heme domain of cytochrome *c*. Apoptosis **19:**259–268. http://dx.doi.org/10.1007/s10495-013-0915-6.
33. **Majumder M, Huang C, Snider MD, Komar AA, Tanaka J, Kaufman RJ, Krokowski D, Hatzoglou M.** 2012. A novel feedback loop regulates the response to endoplasmic reticulum stress via the cooperation of cytoplasmic splicing and mRNA translation. Mol. Cell. Biol. **32:**992–1003. http://dx.doi.org/10.1128/MCB.06665-11.
34. **Skorupa A, King MA, Aparicio IM, Dussmann H, Coughlan K, Breen B, Kieran D, Concannon CG, Marin P, Prehn JH.** 2012. Motoneurons secrete angiogenin to induce RNA cleavage in astroglia. J. Neurosci. **32:**5024–5038. http://dx.doi.org/10.1523/JNEUROSCI.6366-11.2012.
35. **Jeon US, Kim JA, Sheen MR, Kwon HM.** 2006. How tonicity regulates genes: story of TonEBP transcriptional activator. Acta Physiol. (Oxf.) **187:**241–247. http://dx.doi.org/10.1111/j.1748-1716.2006.01551.x.
36. **Yang J, Liu X, Bhalla K, Kim CN, Ibrado AM, Cai J, Peng TI, Jones DP, Wang X.** 1997. Prevention of apoptosis by Bcl-2: release of cytochrome *c* from mitochondria blocked. Science **275:**1129–1132. http://dx.doi.org/10.1126/science.275.5303.1129.
37. **Khandekar N, Willcox MD, Shih S, Simmons P, Vehige J, Garrett Q.** 2013. Decrease in hyperosmotic stress-induced corneal epithelial cell apoptosis by L-carnitine. Mol. Vis. **19:**1945–1956.
38. **Yoshida H, Kong YY, Yoshida R, Elia AJ, Hakem A, Hakem R, Pen-**

ninger JM, Mak TW. 1998. Apaf1 is required for mitochondrial pathways of apoptosis and brain development. Cell **94:**739–750. http://dx.doi.org/10.1016/S0092-8674(00)81733-X.
39. **Goldstein JC, Munoz-Pinedo C, Ricci JE, Adams SR, Kelekar A, Schuler M, Tsien RY, Green DR.** 2005. Cytochrome *c* is released in a single step during apoptosis. Cell Death Differ. **12:**453–462. http://dx.doi.org/10.1038/sj.cdd.4401596.
40. **Novoa EM, Pavon-Eternod M, Pan T, Ribas de Pouplana L.** 2012. A role for tRNA modifications in genome structure and codon usage. Cell **149:**202–213. http://dx.doi.org/10.1016/j.cell.2012.01.050.
41. **Phizicky EM, Hopper AK.** 2010. tRNA biology charges to the front. Genes Dev. **24:**1832–1860. http://dx.doi.org/10.1101/gad.1956510.
42. **El Yacoubi B, Bailly M, de Crecy-Lagard V.** 2012. Biosynthesis and function of posttranscriptional modifications of transfer RNAs. Annu. Rev. Genet. **46:**69–95. http://dx.doi.org/10.1146/annurev-genet-110711-155641.
43. **Von Ahsen O, Waterhouse NJ, Kuwana T, Newmeyer DD, Green DR.** 2000. The "harmless" release of cytochrome *c*. Cell Death Differ. **7:**1192–1199. http://dx.doi.org/10.1038/sj.cdd.4400782.
44. **Emara MM, Ivanov P, Hickman T, Dawra N, Tisdale S, Kedersha N, Hu GF, Anderson P.** 2010. Angiogenin-induced tRNA-derived stress-induced RNAs promote stress-induced stress granule assembly. J. Biol. Chem. **285:**10959–10968. http://dx.doi.org/10.1074/jbc.M109.077560.
45. **Czech A, Wende S, Morl M, Pan T, Ignatova Z.** 2013. Reversible and rapid transfer-RNA deactivation as a mechanism of translational repression in stress. PLoS Genet. **9:**e1003767. http://dx.doi.org/10.1371/journal.pgen.1003767.
46. **Iordanov MS, Ryabinina OP, Wong J, Dinh TH, Newton DL, Rybak SM, Magun BE.** 2000. Molecular determinants of apoptosis induced by the cytotoxic ribonuclease onconase: evidence for cytotoxic mechanisms different from inhibition of protein synthesis. Cancer Res. **60:**1983–1994.
47. **Machnicka MA, Milanowska K, Osman Oglou O, Purta E, Kurkowska M, Olchowik A, Januszewski W, Kalinowski S, Dunin-Horkawicz S, Rother KM, Helm M, Bujnicki JM, Grosjean H.** 2013. MODOMICS: a database of RNA modification pathways—2013 update. Nucleic Acids Res. **41:**D262–D267. http://dx.doi.org/10.1093/nar/gks1007.
48. **Saikia M, Fu Y, Pavon-Eternod M, He C, Pan T.** 2010. Genome-wide analysis of N1-methyl-adenosine modification in human tRNAs. RNA **16:**1317–1327. http://dx.doi.org/10.1261/rna.2057810.
49. **Sadagopan S, Veettil MV, Chakraborty S, Sharma-Walia N, Paudel N, Bottero V, Chandran B.** 2012. Angiogenin functionally interacts with p53 and regulates p53-mediated apoptosis and cell survival. Oncogene **31:**4835–4847. http://dx.doi.org/10.1038/onc.2011.648.
50. **Li S, Yu W, Kishikawa H, Hu GF.** 2010. Angiogenin prevents serum withdrawal-induced apoptosis of P19 embryonal carcinoma cells. FEBS J. **277:**3575–3587. http://dx.doi.org/10.1111/j.1742-4658.2010.07766.x.
51. **Li S, Yu W, Hu GF.** 2012. Angiogenin inhibits nuclear translocation of apoptosis inducing factor in a Bcl-2-dependent manner. J. Cell Physiol. **227:**1639–1644. http://dx.doi.org/10.1002/jcp.22881.
52. **Yuan S, Yu X, Asara JM, Heuser JE, Ludtke SJ, Akey CW.** 2011. The holo-apoptosome: activation of procaspase-9 and interactions with caspase-3. Structure **19:**1084–1096. http://dx.doi.org/10.1016/j.str.2011.07.001.
53. **Bratton SB, Walker G, Srinivasula SM, Sun XM, Butterworth M, Alnemri ES, Cohen GM.** 2001. Recruitment, activation and retention of caspases-9 and -3 by Apaf-1 apoptosome and associated XIAP complexes. EMBO J. **20:**998–1009. http://dx.doi.org/10.1093/emboj/20.5.998.
54. **McIlwain DR, Berger T, Mak TW.** 2013. Caspase functions in cell death and disease. Cold Spring Harb. Perspect. Biol. **5:**a008656. http://dx.doi.org/10.1101/cshperspect.a008656.
55. **National Institutes of Health.** 1985. Guide for the care and use of laboratory animals. NIH publication 85-23. National Institutes of Health, Bethesda, MD.